PAPER

Increased heat dissipation with the X-divertor geometry facilitating detachment onset at lower density in DIII-D

IOP Publishing | International Atomic Energy Agency Nuclear Fusion

Nucl. Fusion **57** (2017) 086017 (10pp) https://doi.org/10.1088/1741-4326/aa7644

Increased heat dissipation with the X-divertor geometry facilitating detachment onset at lower density in DIII-D

B. Covele[1], M. Kotschenreuther[2], S. Mahajan[2], P. Valanju[2], A. Leonard[1], J. Watkins[3], M. Makowski[4], M. Fenstermacher[4] and H. Si[5]

[1] General Atomics, San Diego, CA, United States of America
[2] University of Texas at Austin, Austin, TX, United States of America
[3] Sandia National Laboratory, Albuquerque, NM, United States of America
[4] Lawrence Livermore National Laboratory, Livermore, CA, United States of America
[5] Institute of Plasma Physics, Chinese Academy of Sciences, Hefei, Anhui, People's Republic of China

E-mail: coveleb@fusion.gat.com

Received 16 December 2016, revised 3 May 2017
Accepted for publication 1 June 2017
Published 23 June 2017

Abstract

The X-divertor geometry on DIII-D has demonstrated reduced particle and heat fluxes to the target, facilitating detachment onset at 10–20% lower upstream density and higher H-mode pedestal pressure than a standard divertor. SOLPS modeling suggests that this effect cannot be explained by an increase in total connection length alone, but rather by the addition of connection length specifically in the power-dissipating volume near the target, via poloidal flux expansion and flaring. However, poloidal flaring must work synergistically with divertor closure to most effectively reduce the detachment density threshold. The model also points to carbon radiation as the primary driver of power dissipation in divertors on the DIII-D floor, which is consistent with experimental observations. Sustainable divertor detachment at lower density has beneficial consequences for energy confinement and current drive efficiency for core operation, while simultaneously satisfying the exhaust requirements of the plasma-facing components.

Keywords: X-divertor, detachment, DIII-D, flux expansion, magnetic geometry, divertor

(Some figures may appear in colour only in the online journal)

1. Introduction

Improved confinement and higher core plasma temperatures on the path to fusion ignition exacerbate the problem of heat loading on the tokamak walls, such that the plasma-surface interaction can quickly dictate the efficiency of the entire tokamak. Future tokamaks' heat fluxes may soon push past the mitigation capabilities that radiative and neutral cooling can offer in a standard divertor (SD) geometry. Requiring ever higher densities to bring the divertor into detachment can degrade the H-mode pedestal, compromise core energy confinement, reduce current drive efficiency, and increase the likelihood of disruptions [1].

If detachment at higher density is prohibited for the sake of core performance, it then becomes advantageous to modify the divertor magnetic geometry, with greater connection length and flux expansion. Historically, this has been done to reduce plasma temperatures and increase plasma-wetted area A_w at the divertor target, without additional gas puffing. Wetted area can be increased by poloidal flux expansion, as in the cases of the X-divertor (XD) [2] and Snowflake Divertor (SF) [3], or by combined toroidal and poloidal flux expansion, as in the case of the super X-divertor (SXD) [4]. For the purposes of this paper, 'flux expansion' will refer specifically to poloidal flux expansion, unless otherwise stated.

It is important to note that, due to the relative weakness of B_p compared to B_t, poloidal flux expansion alone does not geometrically reduce the field-parallel heat flux in the SOL, $Q_{\parallel}$, but rather its perpendicular projection on the target, Q_{perp}. Reducing Q_{perp} via poloidal flux expansion is functionally

equivalent to making the target plate more parallel to the total incident field (i.e. reducing $\sin\theta = (B_p/B)\sin\theta_p$, where θ_p is the angle between B_p and the target). Since there are practical limits to the lower bound of θ, the geometric reduction of heat flux by poloidal flux expansion at the target is fundamentally limited for an *attached* plasma. Increased connection length notwithstanding, the usefulness of poloidal flux expansion to reduce T_e and Q_{perp} would now seem to be exhausted, unless we further consider the synergy between divertor magnetic geometry, confined particles, and radiating volume—independent of the local surface projection. After all, the ideal approach to heat flux mitigation is divertor detachment, the condition in which neutrals and photons overtake ions and electrons as the primary power delivery mechanism to the target, such that the plasma-target interaction is greatly reduced. Photons' and neutrals' indifference to the local magnetic field ensures that the persisting heat load is spread more isotropically over the target. Full detachment (i.e. detachment across the entire radial profile) is characterized at the target by: very low electron temperatures (less than 1–2 eV), a strong reduction in the parallel heat flux, a strong reduction in plasma pressure, and eventually a rollover of the plasma density and ion flux.

For the purposes of this paper, 'detachment onset' will refer to the first of these criteria: the reduction of the peak target electron temperature. The temperature criterion tends to be the simplest to identify and characterize in SOL fluid codes, while the more rigorous criteria indicative of deeper detachment, such as ion flux rollover, require more sensitive input parameters to accurately capture, which was out of the scope of this initial modeling effort. The SOLPS models described here do not include density points at which ion flux rollover was observed. Consequently, in the modeling section of this paper (section 3), the focus is on achieving the dissipative environment necessary for detachment onset, rather than characterizing the Degree of Detachment [5] and its evolution, a more ambitious goal. By contrast, divertors on DIII-D routinely exhibit ion saturation current rollover, so in addition to characterizing heat dissipation, experimental observations will be made about the detachment evolution in section 4.

2. Divertor flaring and detachment

Full detachment has been historically elusive as a divertor operating point, as detachment at the required, higher densities tends to cause degradation of the H-mode pedestal and loss of energy confinement in the core. So, while flux expansion is limited in mitigating the heat flux of attached plasmas, it may facilitate detachment onset at lower densities for a given set of plasma conditions. As it is, the SD exhibits a *decrease* in flux expansion as it approaches the target, resulting in an ever-*larger* pitch angle of the total field B. By contrast, a strong XD causes flux expansion to sharply *increase* downstream, resulting in an ever-*smaller* pitch angle toward the target. This increase in flux expansion toward the target is called poloidal flaring, named for the divergent character of the field lines. XDs, with their flux expansion preferentially maximal at the target, are defined by their poloidal flaring [6].

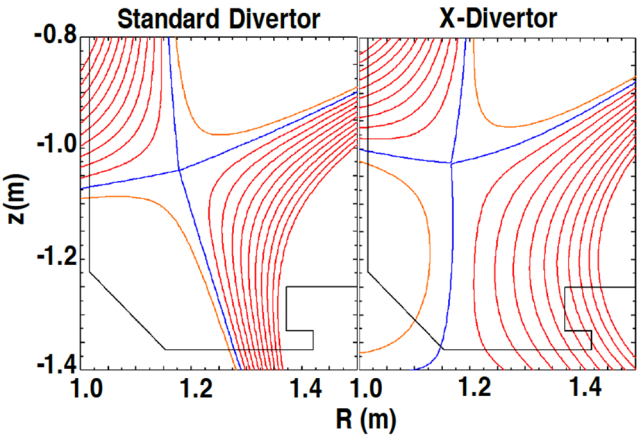

Figure 1. Poloidal cross-sections of CORSICA equilibrium models for the SD and XD on the DIII-D lower floor. The XD creates poloidal flux expansion at the target with a secondary *x*-point very close to the strike point. This has the obvious effect of causing the field lines to diverge near the strike point, but it also adds connection length preferentially in the highly radiating volume near the target.

The XD's poloidal flaring may be useful to increase the *power-dissipating volume* in the divertor, facilitating detachment onset. First, an XD with high flux expansion and shallow pitch angle near the target maximizes ion and electron energy/momentum losses in the volume where neutrals are most dense. Second, sputtered impurity ions can be expected to be better confined near the target, since a greater fraction of the connection length is distributed at the target. Lower-*Z* impurities, such as carbon, can radiate more power when confined near the target.

In summary, it is reasonable to hypothesize that local power/momentum losses in the divertor can be dependent on B_p, in cases where both flux expansion and divertor closure are sufficiently strong to work synergistically. Both collisional neutral losses and impurity radiative losses can indirectly reduce the divertor temperature, pressure, and $Q_{\|}$, encouraging detachment onset for lower neutral pressures, less gas puffing, and lower upstream densities.

Moreover, if the divertor is also highly flared, as is the case for the XD, flux expansion upstream is weaker, and the field pitch is larger through the volume near the core *x*-point. The loss mechanisms are weakened, and $Q_{\|}$ is higher. Thus, in a strong XD, with both flux expansion and poloidal flaring, a gradient in $Q_{\|}$ can be induced from divertor entrance to target, encouraging detachment at the target, yet resisting upstream migration of the detachment front to the core. Upstream migration of the detachment front is not inherently detrimental to core performance; radiation closer to the core's *x*-point ensures that the radiated power is incident over a larger wall area, and operational spaces have been explored with *x*-point radiation and no loss of energy confinement [7]. However, if divertor flaring offers passive resistance to migration of the detachment front, it can slow the real-time progression of the radiation front, widening the response window for active control of the front. A more rigorous study of this possibility has recently been published by Lipschultz *et al* [8].

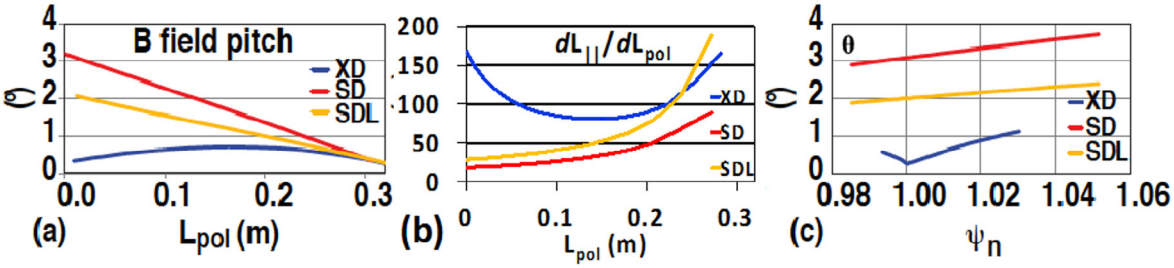

Figure 2. A comparison of the magnetic features of the three divertor models: (*a*) a poloidal profile of field pitch angle through the divertor leg, (*b*) the subsequent distribution of connection length in the divertor leg, and (*c*) the radial profile of the angle θ between the total field and the target. L_{pol} is the distance from the target along the separatrix, and ψ_n is the normalized flux coordinate. The XD (blue) creates large flux expansion very near the target, resulting in a longer electron/ion path length near the target, and a shallower angle of approach. The SDL model mimics the added connection length of the XD by globally scaling the field of the SD model, isolating the effect of connection length.

Flux expansion, coupled with sufficiently large poloidal flaring, may (a) bring about detachment for a lower core Greenwald fraction, and (b) resist the migration of the detachment front upstream to the core, preserving the H-mode pedestal in deeper divertor detachment. To explore the effect of flaring on detachment, XDs with large increases in flux expansion toward the target are required.

The parallel gradient in pressure and $Q_{\|}$ as a result of poloidal flaring in the XD is described as an indirect effect, with momentum/energy loss from dissipative reactions acting as the intermediary. It would be ideal to induce the gradients directly instead, by geometric expansion of the SOL flux tube. This is synonymous with a reduction in B_t, which is only achieved by moving the divertor strike point out to a larger major radius—i.e. the prescription of the SXD. The SXD has previously been promoted as a means to increase target plasma-wetted area. However, for the reasons explained in the context of the XD, we can expect that an SXD would have even greater benefits to detachment onset facilitation, with its combined toroidal and poloidal flaring. But because optimal SXDs tend to require more complicated PF current distributions, XDs may offer a simpler, sufficient approach to detachment facilitation and control. Equilibrium modeling with CORSICA has shown that XDs with large flaring are feasible on several present-day tokamaks [9].

3. XD dissipation modeling with CORSICA and SOLPS

Initial equilibrium and transport modeling of XDs with CORSICA and SOLPS largely motivated XD detachment experiments on DIII-D. These models used simplified input to examine general trends in divertor performance with changes in geometry, to guide the experimental strategy. They stop short of examining detachment in further detail (i.e. the rise of volumetric recombination and ion current rollover), but simply aim to understand how the divertor geometry changes power dissipation.

First, CORSICA free-boundary equilibria (figure 1) acted as the target equilibria for the development of plasma control scenarios. The lower floor was chosen as the strike point location to increase closure, to make more apparent any change the XD geometry made to plasma-neutral interaction or radiation. Next, B2-Eirene, a coupled 2D plasma fluid code with 3D Monte Carlo neutrals [10], was used to compare heat and particle transport of these XD and SD geometries.

In comparing the XD and SD geometries' effect on transport, however, a dilemma emerged. The poloidal flux expansion of XDs engenders two beneficial effects simultaneously: a shallower pitch angle through the radiating volume near the target, and an overall increase in SOL connection length. To distinguish between these effects, a third, artificial geometry was included: the same SD poloidal field geometry, but with B_p scaled down globally to decrease field pitch and match the larger outer midplane connection length of the XD. In this 'hybrid' geometry, hereafter referred to as the SDL geometry, the contribution of added connection length from XD target flux expansion could be isolated, such that any additional benefit to power dissipation seen in the XD model is more likely to be attributable to flaring specifically. The magnetic distinctions of the three geometries are illustrated in figure 2.

Input to SOLPS was chosen to represent typical conditions in DIII-D. Deuterium and carbon species were present. The carbon chemical sputtering yield was fixed at 1% for all material surfaces, while physical sputtering used the Roth-Bohdansky model. The ADAS database [11] was used for reaction cross-sections in B2. The Eirene reaction block used the standard set from SOLPS 5.1 (i.e. Eirene 'facelift') plus neutral–neutral collisions, though there was no immediate evidence that neutral–neutral collisions strongly affected the solutions. Volumetric recombination was included in Eirene, but photons for optically thick plasmas were not included.

Radial heat and particle transport in the three geometries used constant diffusion coefficients, $X\perp = 0.5\ \mathrm{m^2\ s^{-1}}$ and $D\perp = .15\ \mathrm{m^2\ s^{-1}}$, for all species' charge states to simulate a narrow, H-mode-like power SOL width λ_q—about 2 mm. These values were also chosen to ensure that most of the power crossing the separatrix arrived in the divertor, as opposed to the mesh boundary in the far SOL. Anomalous radial viscosity was set nominally to $0.5\ \mathrm{m^2\ s^{-1}}$. While SOLPS is capable of more complex, radially varying transport coefficients to match more realistic experimental conditions, the nature of this initial divertor model comparison motivated a simpler approach to transport. As the comparison of interest is magnetic geometry, it was unclear *a priori*

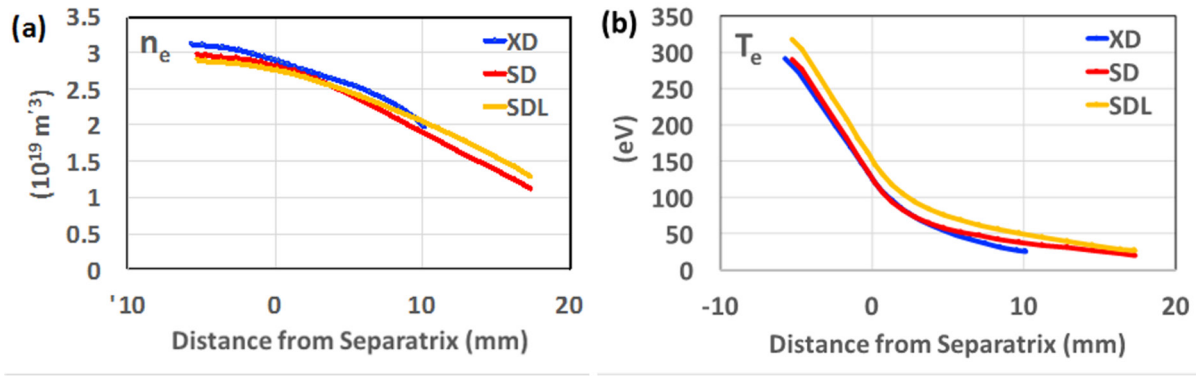

Figure 3. Model electron density (*a*) and temperature (*b*) profiles at the outer midplane for spatially constant $X\perp = 0.5$ m^2 s^{-1} and $D\perp = .15$ m^2 s^{-1} are very consistent between all three divertor geometries. The power SOL width λ_q is ~2 mm. The radial extent of the XD profile is less due to limits on the mesh created by intersecting structures near the target.

how the differences in flux expansion/compression could, in reality, incur changes to the radial transport indirectly, via changes in neutral fueling, impurity transport, etc. Therefore, there was no compelling justification to introduce more free transport parameters—beyond attaining an appropriate λ_q—to match a particular upstream density or temperature profile, particularly prior to the experiment, if the very change in magnetic geometry could feedback on those profiles. Such feedback on the pedestal profile has been observed in divertor closure experiments on DIII-D [12].

SOLPS also permits poloidal variation of the transport coefficients, and research has shown that suitably modest poloidal scaling of the transport coefficients in the divertor is experimentally justified [13]. Relaxation of the transport profile in the divertor broadens the heat flux profile, easing the burden on the target. In this sense, the simpler, fixed-transport models cited in this paper represent a conservative estimate of density thresholds for detachment onset. Following the conclusion of the XD experiment, the inclusion of radially and poloidally varying transport coefficients to match the experimentally measured profiles remains an important part of future work.

Total input power across the core boundary was 5 MW, equally shared between ions and electrons, to simulate 5.5 MW of NB heating, with 0.5 MW of core radiation. A constant-particle-flux condition was enforced at the core boundary, with an external, constant D_2 gas puff fueling the core density from the crown of the plasma. This condition ensures stable, steady-state conditions at the boundary, while also allowing the core density to evolve in response to the external neutral fueling, which may or may not be an explicit relationship. A very weak pumping surface (1% absorption) was introduced at the midplane to achieve global particle balance without strongly affecting the local divertor neutral density.

While drift terms can be implemented in the SOLPS 5.1 transport model, this has frequently led to numerical stability problems addressed in later code versions [14]. Therefore, no drift terms are applied in this simplified model. The inclusion of drifts can be expected to shift the power balance between inner and outer targets, and should be considered for future XD modeling work. At the higher divertor densities approaching detachment onset considered here, it is expected that drift effects will not qualitatively change the trends sought.

When comparing different divertor geometries, there were two ways identified to assess benefits to power dissipation: (1) compare the divertors' target conditions for the same upstream conditions, or (2) compare the divertors' required upstream conditions to achieve the same target conditions. The first assessment informs how the divertors behave differently due to their geometries, and the second assessment informs how the core may be differently affected to achieve similar dissipation in each divertor. Both assessments are done in turn.

First, we inspect the upstream density threshold for detachment onset, defined here as the point where the peak target temperature is about 1–2 eV. For the given upstream profiles of figure 3, figure 4 summarizes the conditions of the three divertor geometries' target profiles with similar upstream profiles and separatrix density ($n_{e,sep}$) of 2.7×10^{19} m^{-3}, where the XD is at detachment onset. All target profiles are plotted against normalized poloidal flux, to act as a standard radial coordinate along the target surface, despite the much larger heat footprint that the XD's flux expansion creates in real space. Figure 4 clearly shows the advanced state of power and momentum dissipation at the XD target, compared to the SD or SDL targets. Comparing the SD and SDL geometries in these models, extra connection length has shown some modest benefit to electron temperature reduction, but cannot fully account for the dissipation exhibited by the XD.

Next, we examine the consequences of high dissipation to the poloidal gradients in the divertor geometries, where the accompanying upstream conditions are compared when all three divertor targets have similarly reduced peak electron temperatures. Ideally, the divertor should achieve low temperatures and heat at the target while maintaining high values upstream, for better core performance. Figure 5 is a collection of poloidal profiles of the three divertors with cold target electron temperatures. Note the different $n_{e,sep}$ for which these target conditions occur in each geometry: 2.7×10^{19} m^{-3} for the XD, 3.5×10^{19} m^{-3} for the SD, and 3.1×10^{19} m^{-3} for the SDL.

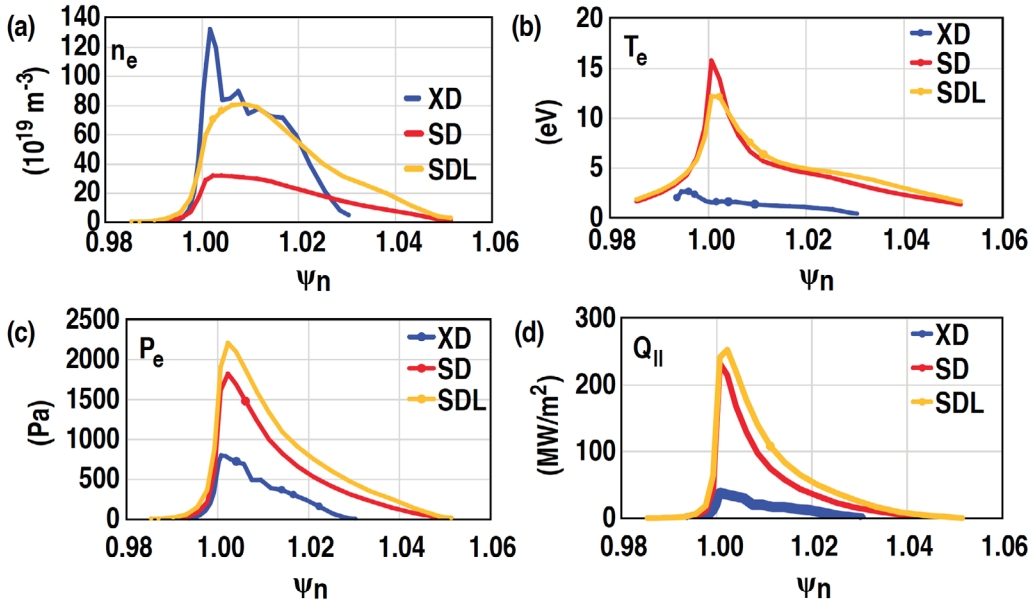

Figure 4. Despite similar model upstream profiles, target profiles for the SD, SDL, and XD geometries are very different. The XD exhibits a stronger degree of dissipation at the target with higher densities (*a*), lower temperatures (*b*), lower electron pressure (*c*), and lower parallel heat flux (*d*). The increased dissipation of the XD can be explained possibly by the very shallow *B*-field angle through the dissipative volume with flux expansion.

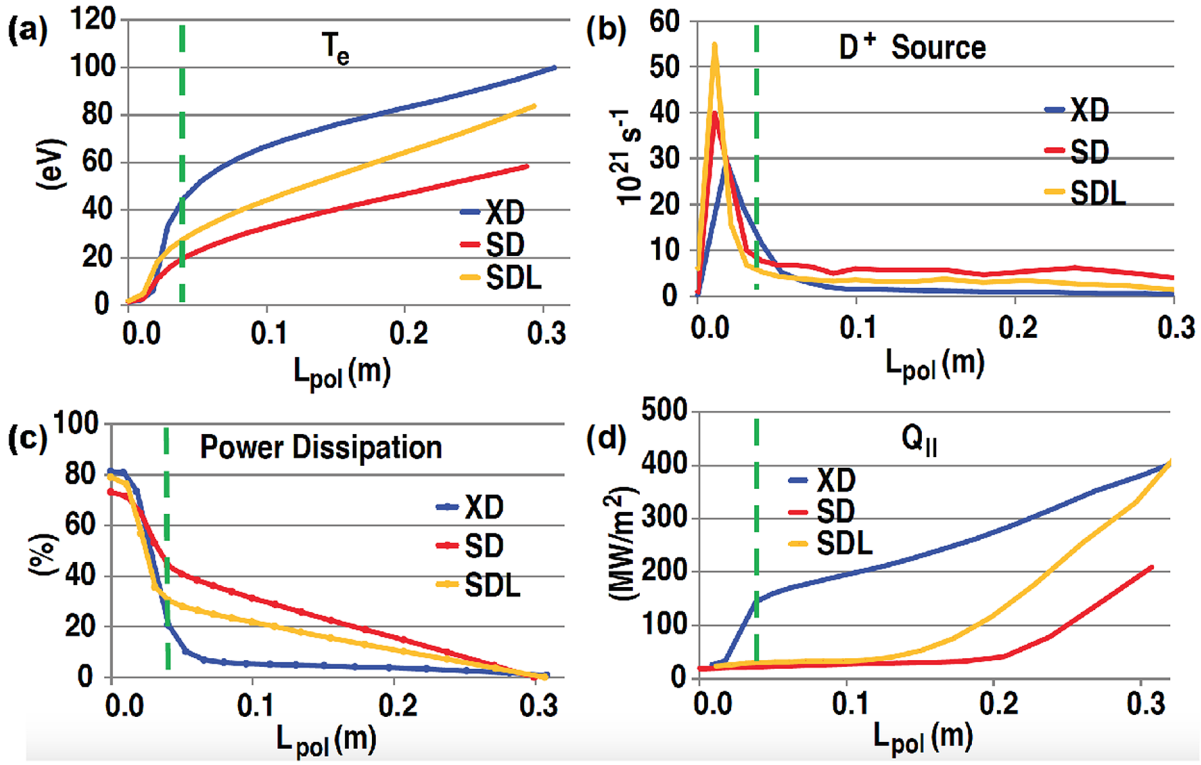

Figure 5. SOLPS poloidal profiles for the SD, SDL, and XD geometries in a similar state of detachment. L_{pol} is the distance along the poloidal field line to the target. The vertical, dashed line indicates the leading edge of the ionization front, identified as the location where ionization sharply increases before crashing at the target. Greater flux expansion at the XD target distributes a greater portion of the total connection length at the target, so while the ionization front (b) of all three geometries is similarly located (albeit for significantly different densities), the XD dissipates its power much closer to the target (c), resulting in very steep poloidal gradients in T_e (a) and $Q_{||}$ (d), and better insulation between the target and the core upstream.

The radial locations for these 1D profiles were chosen based on the location of the peak values at the divertor entrance. While the ionization fronts for all three geometries are similarly located (5(*b*)), the XD dissipates nearly all of its power near the target (5(*c*)), which may be attributable to its flaring (2(*a*)) and greater distribution of connection length $dL_{||}$ near the target (2(*b*)). This results in much steeper gradients in temperature and $Q_{||}$ (5(*a*) and (*d*)), as expected. It was also found that

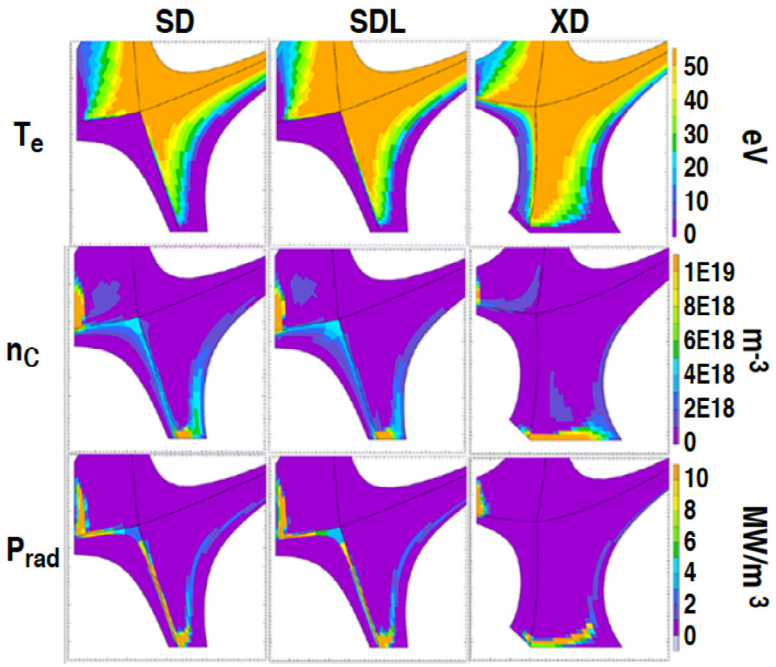

Figure 6. SOLPS 2D color plots of electron temperature, carbon impurity concentration, and radiated power in the SD, SDL, and XD geometries on the verge of detachment. The XD reduces its temperature in a volume much closer to the target. Carbon impurities in the XD are also better confined to the target region at detachment onset. Lower neutral pressures and a larger allocation of connection length at the XD target prevent carbon neutrals from migrating upstream at this density, before being ionized and pushed back downstream. Higher neutral pressures at higher densities required for detachment in the SD and SDL geometries allow carbon to travel upstream and radiate at the core *x*-point.

the local target neutral densities required to achieve these cold temperatures were 5 times lower in the XD model. Thus, the XD model not only detached at lower electron density (figures 3 and 4), but it also more effectively resisted volumetric losses closer to the core, insulating the core from the target (figure 5).

Additionally, we examined carbon impurity concentrations and subsequent radiation patterns at detachment onset, as one would see from a bolometer. The XD more effectively restricted carbon impurities near the target at detachment onset, while the SD and SDL geometries allowed higher carbon concentrations near the core *x*-point (figure 6). Quantitatively, we see in figure 7 that carbon radiation was the primary driver of power loss in this XD model. Recent research by Krasheninnikov *et al* has also observed and offered explanation for the dominant role of impurity radiation in divertor power dissipation [15]. The XD's peak carbon radiative losses were 30% higher than those of the SD. It is unclear at this time how strongly the choice of baffling in other models may affect the ratio between carbon radiation, neutral radiation, and collisional loss mechanisms like charge exchange.

Different choice of baffling may alter how power is dissipated in the divertor, but what's clear from the modeling is that closure is a necessary ingredient for enhancing XD power/momentum dissipation. Analogous SD/XD models run on DIII-D's open lower shelf showed no significant difference in power dissipation leading to detachment onset. Despite the presence of target flux expansion, neutral trapping was too weak for ions/electrons to cool along the additional path length. For brevity, these results are not explicitly included here, only the divertor models on the lower floor with higher closure.

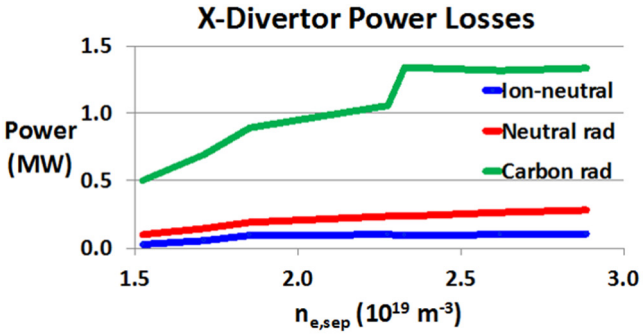

Figure 7. Integrated volumetric power losses in the XD due to carbon radiation, neutral radiation, and ion-neutral interactions as a function of upstream density. Carbon radiation is clearly the primary driver of power loss. The XD exhibited 30% greater peak carbon radiative losses than the SD at high density.

In summary, the XD model much more effectively reduced heat fluxes and temperatures at the target at lower density than either the SD or SDL models (figure 8). The SDL model, whose midplane connection length matched the XD, suggests that the XD's improved dissipation is not explained merely by added connection length due to flux expansion. Rather, the distribution of flux expansion and connection length preferentially at the target encourages dissipation downstream, and discourages it upstream. Close inspection of the power loss mechanisms confirmed that XD's poloidal flaring can be just as important—if not more important—to impurity confinement as it is to enhanced plasma-neutral interaction in closed divertors.

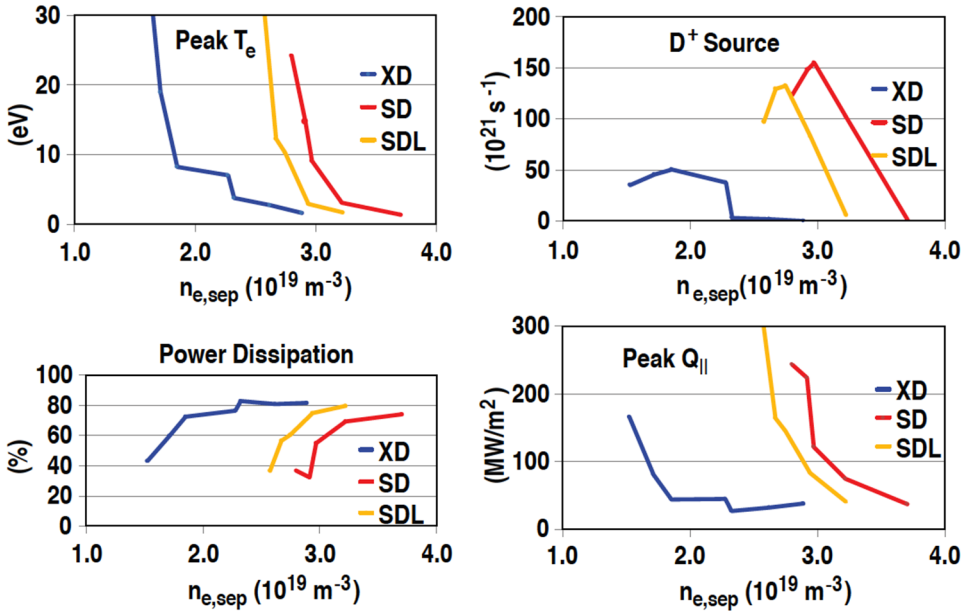

Figure 8. The XD model reduces temperatures, heat flux intensity, ions, and total power at a significantly lower density than either the SD or SDL models. XD detachment facilitation cannot be explained solely by greater total connection length, but rather a redistribution of connection length near the target via flux expansion.

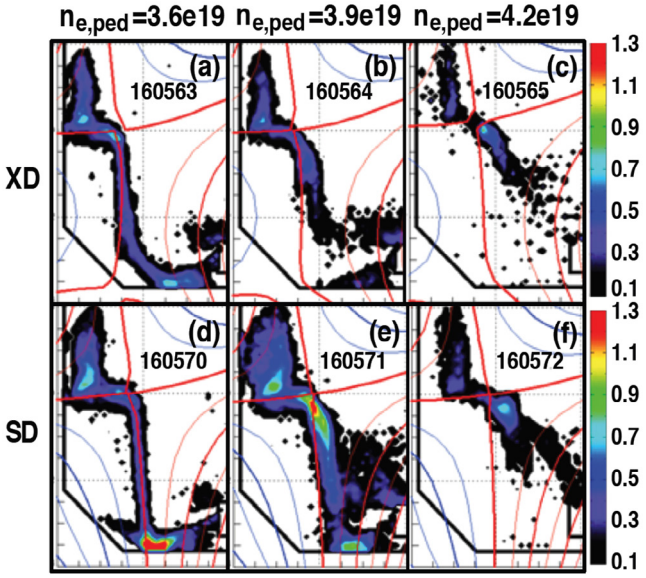

Figure 9. Very low target T_e is the first predictor of detachment onset. C^{2+} emissions can be used to track the location of the temperature front for the XD (*a*)–(*c*) and the SD (*d*)–(*f*) at incremental pedestal densities. At the lowest density, the XD detachment front begins to peel away from the target ((*a*), circled), while the SD remains firmly attached ((*d*), circled). At higher density, the XD is completely detached (*b*), with the SD still showing strong emissions at the target (*e*). At the highest density, both divertors (*c*) and (*f*) are finally fully detached.

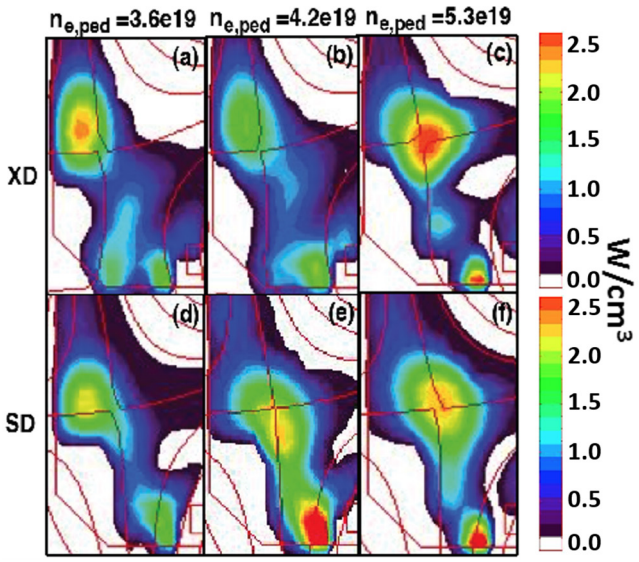

Figure 10. During detachment, bolometer reconstructions show the regions in the outer divertor leg where radiation is strongest (the strongly radiating inner leg, already detached, can be disregarded). At lowest densities, the XD radiating volume (a) is similar to that of the SD (d). At higher density, the XD's radiating volume in the outer leg stays near the target (*b*), while the SD begins to radiate throughout the outer divertor volume (*e*). This is consistent with the idea that the XD's poloidal flaring can discourage upstream volumetric losses, preventing the migration of the detachment front, until at very high density both geometries exhibit strong radiation near the *x*-point (*c*) and (*f*).

4. Experimental results for XD heat dissipation and detachment onset

To test the benefits of divertor flaring to heat dissipation suggested in the models of section 3, XD geometries were created alongside SDs, for the same lower single-null H-mode plasma, in an experiment on DIII-D. Unlike the modeling strategy, which was limited to achieving the weakest condition for detachment onset—low electron temperatures—the experimental geometries could be deeply detached, to examine the effect on the pedestal.

Following the conclusions of the model trends, an XD was created at high plasma triangularity, such that the strike point resided on the lower floor, where closure was higher.

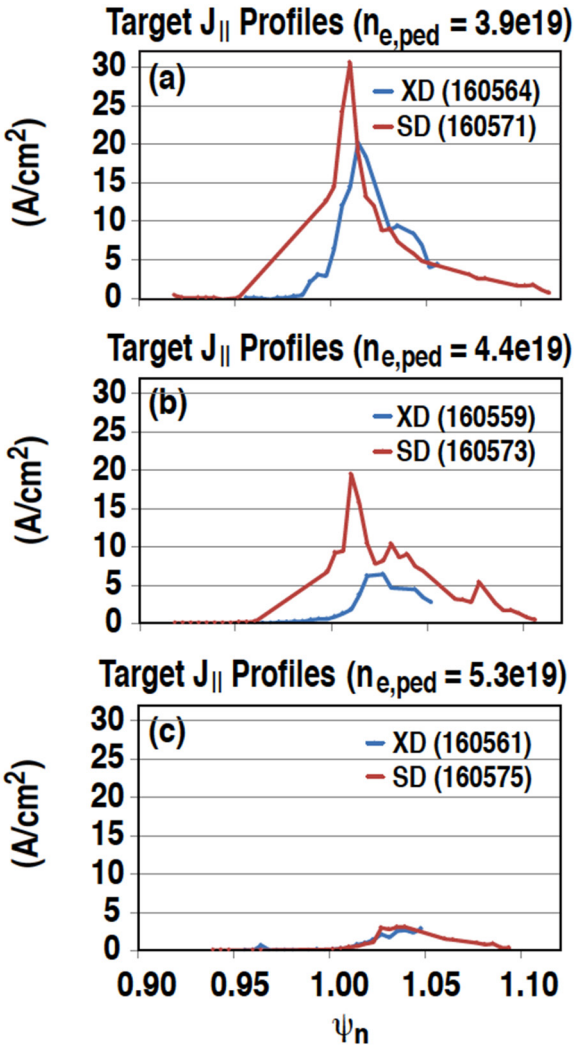

Figure 11. Comparison of three pairs of XD/SD shots' target profiles of parallel ion current at progressively higher pedestal densities. At lower densities (left and middle plots), the XD exhibits ion current reduction ahead of the SD. At very high densities (right plot), the two profiles finally exhibit similar ion current reduction. The values plotted ($J_{\|}$ versus ψ_n) normalize for any geometric projection of the flux tube on the target, so the XD's lower ion current is a result of advanced detachment, and not merely an increase in plasma-wetted area.

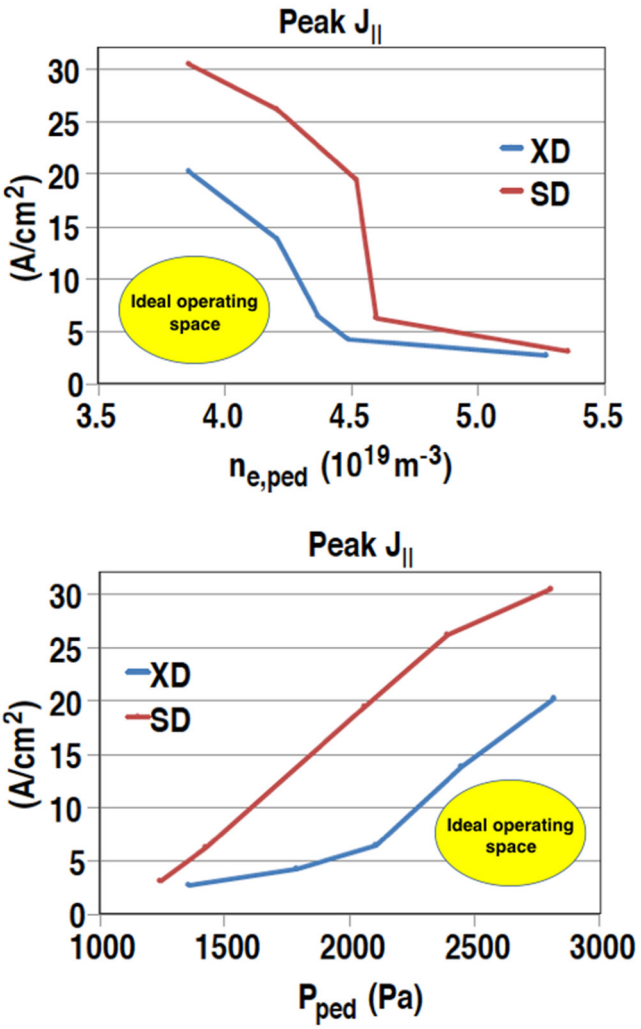

Figure 12. The XD exhibits greater reduction in downstream ion current for lower upstream pedestal densities and higher pedestal pressures (*x*-axes). Effective divertors will seek to lower exhaust heat and particle fluxes while maintaining lower upstream densities and higher pedestal pressures.

An analogous SD was created for reference, with identical beam power, plasma current, elongation, triangularity, and core *x*-point location. Indeed, these geometries were intended to match the model geometries analyzed in figures 1–8. The XD's secondary *x*-point was brought very close to the strike point, strongly increasing the flux expansion at the target. Over several successive shots, a density scan was performed for both divertor geometries, until ultimately the H-mode pedestal pressure was significantly degraded. The twofold motivation for this type of density scan is analogous to our previous assessment of modeling output: (a) to determine the relative densities at which the divertors reached detachment onset, and (b) to characterize the incidental upstream conditions when the divertors are similarly cold.

On the DIII-D lower floor, detachment diagnostics consisted of target Langmuir probes for ion current, an IR camera for heat flux, a tangential camera filtered for C^{2+} emission lines, and bolometer arrays available for 2D reconstructions of radiation. While probes can also be used to infer plasma density and temperature as well, the interpretation of these values becomes more ambiguous at the low temperatures characteristic of detachment onset. Carbon emissions were therefore relied upon to estimate T_e in the divertor leg. Thomson scattering was available upstream to measure midplane electron density and temperature profiles.

Figure 9 shows side-by-side images of C^{2+} emissions from the tangential camera for the XD and SD at the same densities. C^{2+} is a sharp function of electron temperature and radiates strongly in a range of 10–12 eV. The models of figure 5 previously showed how sharply carbon radiation decreases at the target at low temperatures, which the experimental images seem to corroborate. At lowest density in the left column of figure 9, the radiation front of the XD is already peeling away from the target (figure 9(*a*)), signaling onset of partial detachment; meanwhile, the SD is still strongly radiating at the strike point (figure 9(*d*)), indicating higher electron temperatures

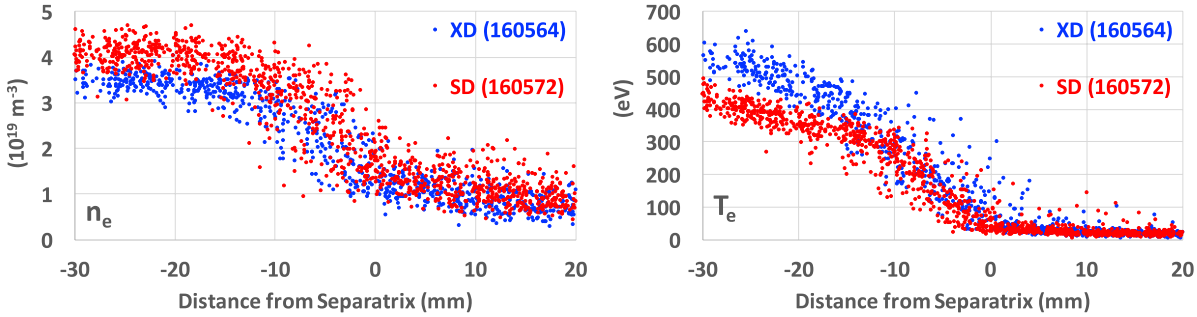

Figure 13. Upstream electron density (left) and temperature (right) profiles for the XD (blue) and the SD (red) with similarly cold temperatures at the target, as determined by the C^{2+} emissions in figure 9. The profiles show a noticeable, albeit modest, difference in pedestal density and temperature, while the data scatter at the EFIT-calculated separatrix makes comparing $n_{e,sep}$ and $T_{e,sep}$ more ambiguous. Using a power accounting method to define the separatrix, the reduction in $n_{e,sep}$ for the XD is 10–20%.

present. At higher density in the center column, almost all carbon radiation has been arrested at the XD target, indicating cold temperatures downstream, with warmer temperatures persisting upstream in an interim state of detachment (9(*b*)). At highest density in the right column, both divertors are now completely detached. However, it is noteworthy that no interim state of detachment was observed for the SD in going from figures 9(*e*)–(*f*), which is consistent with other experimental results on DIII-D. The XD's interim detachment state may be indicative of passive resistance of the detachment front due to flaring.

Figure 10 also illustrates how, as density is increased, the XD's total radiating volume persists longer at the target, before finally migrating to the core *x*-point. By contrast, the radiating volume of the SD is quick to fill the outer divertor leg in addition to the target region. This experimental observation is qualitatively similar to the model profiles of power dissipation in figure 5, where the gradients in $Q_{\parallel}$ were shallower for the SD.

Figure 11 shows conditions locally at the target via probe J_{sat} measurements, where the XD leads the SD in reduction of ion flux to the target at high densities. The plots have been normalized for flux expansion, with a normalized flux coordinate on the abscissa and a parallel current on the ordinate. Because of this normalization, the XD's lower ion current represents a real reduction in the incident ion flux at detachment onset, and not simply a larger projection of the ion flux area on the target due to poloidal flux expansion. Because the experimental divertors were puffed into deep detachment, additional information about the pedestal response to detachment could be examined. Figure 12 summarizes the measured target quantities as a function of $n_{e,sep}$ and P_{ped}, where the XD curve is closer to the ideal operating space: low density, high pedestal pressure, and low target fluxes.

Both the C^{2+} emission and probe data seem to indicate detachment onset for the XD. However, the significant flux expansion from the secondary *x*-point raises the concern that these measurements could be the result of local hot spot formation elsewhere around the torus, due to the very low incident field angle with the target. This is unlikely, however, based on the coverage of the IR and tangential cameras, which can view over 75% of the lower divertor floor around the torus. No such hot spots were observed in the recorded images when measurements were analyzed.

In an attempt to make a judicious comparison between upstream densities of detached XDs and SDs, the upstream profiles of Shots 160564 (XD) and 160572 (SD) were examined. Thomson scattering was used to take these measurements. In these shots, the C^{2+} emissions show unambiguously cold temperatures at the target in figure 9. Figure 13 shows the corresponding upstream profiles under these cold divertor conditions. Trendlines are absent to better show the data scatter and ambiguity near the separatrix. The profiles of figure 13 show that the XD (blue data) dissipates power at slightly lower pedestal density than the SD (red data), but maintains significantly higher pedestal temperatures.

Note that while the model geometries were compared for a given $n_{e,sep}$, in the experiment they are compared for a given $n_{e,ped}$. The separatrix location in the plots of figure 13 is based on the reconstruction of the magnetic field from the EFIT code, but the exact location of the separatrix—and subsequent relation of $n_{e,ped}$ to $n_{e,sep}$—is ambiguous. This further complicates the process of comparing the modeling results directly to the experimental results, in addition to the simplified modeling input used. One consistent method for defining the separatrix location is to examine power accounting, such that the power across the chosen boundary is equal to the power flowing to the divertor [16]. Using this approach to define the separatrix, the reduction in $n_{e,sep}$ to achieve low temperatures in the XD was 10–20% (from 1.9×10^{19} in the SD to 1.5×10^{19} m^{-3} in the XD). This is qualitatively consistent with SOLPS modeling (section 3), which predicted a reduction of 23% in $n_{e,sep}$ (from 3.5×10^{19} in the SD to 2.7×10^{19} m^{-3} in the XD) for detachment onset of the XD.

Though the trend in density reduction to reduce target tempertures and heat fluxes was similar, SOLPS predicted much higher values for the actual density threshold $n_{e,sep}$ (3.5×10^{19} for SD and 2.7×10^{19} m^{-3} for XD). One certainly expects some level of discrepancy due to the simplified transport input used in the model. However, other SOLPS models more closely aligned to experimental data also exhibit a persisting discrepancy. Related research, such as the work of Canik *et al* [17], is ongoing to explain the universal discrepancy seen in the exact detachment density between experiments and the most widely used fluid SOL codes.

Finally, to test the conclusion from the modeling that closure is important to the XD effect, XDs were also generated on the DIII-D lower shelf, a horizontal target with virtually

no closure. As in the modeling, the detachment threshold for these XDs was indistinguishable from similar SDs, despite large flux expansion at the target. For the sake of brevity, this null result is not reported explicitly here, but is an important observation to note for future work.

5. Conclusions

The first XD experiment on DIII-D has shown promise that target flux expansion and flaring can lower the detachment density threshold (here, estimated at 10–20%), which is important for core operational compatibility with proper exhaust power and particle handling. Equally importantly, the experiment has shown XD detachment at higher pedestal *pressure*, which allows the core to maintain higher energy confinement. More refined experiments need to be planned to better resolve the change in the detachment threshold. Future use of divertor Thomson scattering in more closed divertors can better follow the changes in divertor temperatures. The trends in the SOLPS models offer a possible explanation of these experimental observations, by showing how, at the same separatrix density and with identical transport parameters, XDs and SDs differently dissipate energy and momentum in the divertor volume due to their geometries. However, both the models and experimental data indicate that poloidal flux expansion and flaring must work in tandem with divertor closure to see a lower density threshold for detachment onset, whether to better confine radiating impurities, neutrals, or both. Therefore, future experiments can build on the potential benefits of magnetic flaring to detachment onset by (a) enhancing neutral compression at the target; (b) improving strike point and flux expansion precision with secondary *x*-point control; (c) introducing low-Z impurities in the divertor, appropriate for low-temperature radiation; and (d) considering target toroidal and poloidal flux expansion with SXDs.

Acknowledgments

The author wishes to express his gratitude for the strong collaborative effort between the University of Texas Institute for Fusion Studies, the Boundary Center at General Atomics, and the DIII-D experimental team, without which this project would not have been possible.

This work was funded by U.S. DOE contract numbers DE-FC02-04ER54698, DE-FG02-04ER54754, DE-FG03-96ER54366, DE-AC52-07NA27344, and DE-AC04-94AL85000, and by the National Natural Science Foundation of China, contract numbers 11505234 and 11347113. DIII-D data shown in this paper can be obtained in digital format by following the links at https://fusion.gat.com/global/D3D_DMP.

References

[1] Greenwald M. *et al* 1988 A new look at density limits in tokamaks *Nucl. Fusion* **28** 2199
[2] Kotschenreuther M. *et al* 2004 Scrape off layer physics for burning plasmas and innovative divertor solutions *Proc. 20th Int. Conf in Fusion Energy (Vilamoura, Portugal, 1–6 November 2004)* [CD-ROM] (Vienna: IAEA) (http://www-naweb.iaea.org/napc/physics/fec/fec2004/datasets/index.html) (http://www.iaea.org/inis/collection/NCLCollectionStore/_Public/36/080/36080682.pdf)
[3] Ryutov D.D. 2007 Geometrical properties of a 'snowflake' divertor *Phys. Plasmas* **14** 064502
[4] Valanju P.M. *et al* 2009 Super-X divertors and high power density fusion devices *Phys. Plasmas* **16** 056110
[5] Loarte A. *et al* 1998 Plasma detachment in JET Mark I divertor experiments *Nucl. Fusion* **38** 331
[6] Kotschenreuther M. *et al* 2013 Magnetic geometry and physics of advanced divertors: the X-divertor and the snowflake *Phys. Plasmas* **20** 102507
[7] Bernert M. *et al* 2017 Power exhaust by SOL and pedestal radiation at ASDEX upgrade and JET *Nucl. Mater. Energy* (https://doi.org/10.1016/j.nme.2016.12.029)
[8] Lipschultz B. *et al* 2016 Sensitivity of detachment extent to magnetic configuration and external parameters *Nucl. Fusion* **56** 056007
[9] Covele B. *et al* 2014 An exploration of advanced X-divertor scenarios on ITER *Nucl. Fusion* **54** 072006
[10] Schneider R. *et al* 2006 Plasma edge physics with B2-eirene *Contrib. Plasma Phys.* **46** 3–191
[11] Summers H.P. *et al* 2007 ADAS: atomic data, modelling and analysis for fusion *AIP Conf. Proc. (Meudon, France, 15–19 October 2006)* ed E. Roueff vol 901 (New York: AIP) (http://aip.scitation.org/doi/abs/10.1063/1.2727374)
[12] Moser A. *et al* 2016 Effect of divertor closure on pedestal fueling and divertor detachment onset in DIII-D *22nd Int. Conf. on Plasma Surface Interactions (Rome, 30 May–3 June 2016)* (*Nucl. Mater. Energy*) (http://www.psi2016.enea.it/PSI_BOA/Abstracts/184_AL_Moser_abstract_v2.pdf)
[13] Chankin A.V. *et al* 2006 SOLPS modelling of ASDEX upgrade H-mode plasma *Plasma Phys. Control. Fusion* **48** 839
[14] Rozhansky V. *et al* 2009 New B2SOLPS5. 2 transport code for H-mode regimes in tokamaks *Nucl. Fusion* **49** 025007
[15] Krasheninnikov S.I. *et al* 2016 Divertor plasma detachment *Phys. Plasmas* **23** 055602
[16] Stangeby P.C. *et al* 2015 Identifying the location of the OMP separatrix in DIII-D using power accounting *Nucl. Fusion* **55** 093014
[17] Canik J.M. *et al* 2015 Modeling of detachment experiments at DIII-D *J. Nucl. Mater.* **463** 569–72